# The effect of the cation substitution on the structural and vibrational properties of Cs2NaGaxSc(1−x)F6 solid solution.

**ARTICLE** *in* THE JOURNAL OF CHEMICAL PHYSICS · SEPTEMBER 2004

Impact Factor: 2.95 · DOI: 10.1063/1.1773772 · Source: PubMed



**5 AUTHORS**, INCLUDING:

Antonio Carlos Doriguetto
Universidade Federal de Alfenas
**119** PUBLICATIONS **893** CITATIONS
SEE PROFILE

Paulo Sergio Pizani
Universidade Federal de São Carlos
**248** PUBLICATIONS **4,318** CITATIONS
SEE PROFILE

Y. P. Mascarenhas
University of São Paulo
**200** PUBLICATIONS **1,687** CITATIONS
SEE PROFILE

Javier Ellena
University of São Paulo
**405** PUBLICATIONS **2,656** CITATIONS
SEE PROFILE

# The effect of the cation substitution on the structural and vibrational properties of $Cs_2NaGa_xSc_{1-x}F_6$ solid solution

A. C. Doriguetto
*Departamento de Fisica e Informatica, Instituto de Fisica de Sao Carlos, Universidade de Sao Paulo, Caixa Postal 369, CEP 13560-970, Sao Carlos, SP, Brazil*

T. M. Boschi and P. S. Pizani
*Departamento de Fisica, Universidade Federal de Sao Carlos, Caixa Postal 676, CEP 13565-905 Sao Carlos, SP, Brazil*

Y. P. Mascarenhas and J. Ellena
*Departamento de Fisica e Informatica, Instituto de Fisica de Sao Carlos, Universidade de Sao Paulo, Caixa Postal 369, CEP 13560-970, Sao Carlos, SP, Brazil*

(Received 16 February 2004; accepted 25 May 2004)

Raman scattering and x-ray diffration were used to characterize the structural and vibrational properties of the $Cs_2NaGa_xSc_{1-x}F_6$ solid solutions, for $x$ ranging from 0.0 to 1.0. The Raman spectra, taken at room and low temperature, allow us to follow the phase evolution in detail and indicate the breaking of the local symmetry since low Ga concentration levels. Five compositions were studied by x-ray diffraction: $x=0.0$, 0.2, 0.5, 0.8, and 1.0. A cubic space group, $Fm\bar{3}m$, was found to $x=0.0$ and $x=0.2$ and a trigonal one was found to $x=0.5$, 0.8, and 1.0. Details of both phases are presented and the correlation between x-ray diffraction and Raman scattering is discussed. © *2004 American Institute of Physics.* [DOI: 10.1063/1.1773772]

## I. INTRODUCTION

Several compounds possessing the general formula $A_2BMX_6$ crystallize with the elpasolite structure, the name given to the mineral with chemical formula $K_2NaAlF_6$ discovered in 1883.[1] Elpasolite can be considered as an ordered perovskite and is the subject of many studies due to its scientific-technologic importance. Considering the general formula $A_2BMX_6$, $X$ is a onefold valence anion, $A$ and $B$ are onefold valence cations, and $M$ is a threefold valence cation. $X$ is restricted to $F^-$, $Cl^-$, $Br^-$, and $CN^-$ anions. Several cations can occupy the $A$, $B$, and $M$ sites in the chemical formula. The more common $A$ and $B$ cations are $Li^+$, $Na^+$, $K^+$, $Rb^+$, $Cs^+$, $Tl^+$, $NH_4^+$, and $Ag^+$. The $M$ cations are commonly $Al^{3+}$, $Sc^{3+}$, $V^{3+}$, $Cr^{3+}$, $Fe^{3+}$, $Ga^{3+}$, $Y^{3+}$, $In^{3+}$, $Ln^{3+}$, and $Bi^{3+}$. Besides the several combinations of varying anions and cations, it is also possible to form solid solutions, in which $X$, $A$, $B$, and $M$ can represent more than one chemical element.

Many elpasolites crystallize in the space group $Fm\bar{3}m$.[2] However, distortions in the cubic prototype can be induced applying pressure, varying the temperature, and changing the atoms. The stability range of the $A_2BMX_6$ elpasolite structures is given by the Goldschmidt's tolerance factor $t$, used originally to characterize perovskites, which is defined by[3]

$$t=\frac{\sqrt{2}(R_A+R_X)}{(R_M+R_B+2R_X)},$$

where $R_A$, $R_B$, $R_M$, and $R_X$ are the ionic radii of the correspondent ions in the general formula.

The most common elpasolite structures are the fluorides $A_2BMF_6$. These fluorides are expected to occur with the elpasolite structure if $t$ yields a value within the range $0.76 \leqslant t \leqslant 1.13$.[4,5] It has been also shown that the cubic phase is stable for fluorides in the range $0.88 \leqslant t \leqslant 1.0$.[6] For $t>1$, the elpasolites exhibit phases with hexagonal or rhombohedral symmetry. For $t<0.88$, the symmetry decreases to orthorhombic or monoclinic. Therefore these materials are very interesting, since the appropriate combination of cations can lead to different crystalline phases.

These materials often are doped with $3d$ transition elements or rare earth due to their great interest for the manufacturing of tunable solid-state lasers.[8,9] Therefore it is interesting to grow elpasolites with good crystalline quality, looking for the enhancement of the quality of these lasers, which is possible by controlling the type of structure. As the vibrational spectra are sensitive to structural changes, such as structural phase transitions or changes in the symmetry, Raman spectroscopy is a very useful technique to probe local symmetry changes while x-ray diffraction (XRD) is a suitable technique for the determination and refinement of the crystal structure and the lattice symmetry of single crystals.[6–9] Since the splitting of the electronic energy levels due to the crystal field, responsible for the optical properties, is strongly dependent of the site symmetry, here we studied the influence of the cation substitution on the structural and vibrational properties of the solid solutions $Cs_2NaGa_xSc_{1-x}F_6$, with $x$ varying from 0.0 to 1.0, using single-crystal x-ray diffraction and Raman scattering.

## II. EXPERIMENT

Single crystals of the substitutional series $Cs_2NaGa_xSc_{1-x}F_6$ were grown using the hydrothermal method, synthesized from aqueous solutions under elevated

TABLE I. Crystal data and structure refinement results for the substitucional series $Cs_2NaGa_xSc_{1-x}F_6$.

| | $x=0.0$ | $x=0.2$ | $x=0.5$ | $x=0.8$ | $x=1.0$ |
|---|---|---|---|---|---|
| Empirical formula | $Cs_2NaScF_6$ | $Cs_2NaGa_{0.2}Sc_{0.8}F_6$ | $Cs_2NaGa_{0.5}Sc_{0.5}F_6$ | $Cs_2NaGa_{0.8}Sc_{0.2}F_6$ | $Cs_2NaGaF_6$ |
| Space group | $Fm3m$ | $Fm3m$ | $R3m$ | $R3m$ | $R3m$ |
| Unit-cell dimensions/Å | $a=8.867(1)$ | $a=8.8458(5)$ | $a=6.3120(1)$<br>$c=30.744(1)$ | $a=6.2614(3)$<br>$c=30.389(2)$ | $a=6.2570(4)$<br>$c=30.301(2)$ |
| Volume/Å$^3$ | 697.1(2) | 692.17(7) | 1060.77(6) | 1031.8(1) | 1027.4(1) |
| $Z$ | 4 | 4 | 6 | 6 | 6 |
| Absorption coefficient mm$^{-1}$ | 11.444 | 12.109 | 12.707 | 13.943 | 14.592 |
| Crystal size/mm$^3$ | 0.04×0.02×0.02 | 0.03×0.02×0.02 | 0.08×0.06×0.04 | 0.06×0.06×0.05 | 0.06×0.06×0.0 |
| Reflections collected | 1246 | 3870 | 6974 | 5431 | 3703 |
| Independent reflections | 78 | 76 | 437 | 427 | 423 |
| $R$ (int) | 0.0662 | 0.0531 | 0.0837 | 0.0748 | 0.0588 |
| Data/restraints/parameters | 78/0/8 | 76/0/8 | 437/1/29 | 427/4/31 | 423/0/27 |
| Extinction coefficient | 0.003(1) | 0.006(2) | 0.0012(2) | 0.0003(1) | 0.0096(4) |
| Goodness of fit on F$^2$ | 1.241 | 1.226 | 1.344 | 1.111 | 1.119 |
| Final $R$ indices $[I>2\sigma(I)]$ | $R_1=0.0355$ | $R_1=0.0115$ | $R_1=0.0195$ | $R_1=0.0239$ | $R_1=0.0202$ |
| | $wR_2=0.0940$ | $wR_2=0.0279$ | $wR_2=0.0396$ | $wR_2=0.0591$ | $wR_2=0.0426$ |
| $R$ indices (all data) | $R_1=0.0431$ | $R_1=0.0136$ | $R_1=0.0232$ | $R_1=0.0282$ | $R_1=0.0257$ |
| | $wR_2=0.1060$ | $wR_2=0.0287$ | $wR_2=0.0654$ | $wR_2=0.0615$ | $wR_2=0.0575$ |
| Largest diff. peak and hole/e Å$^{-3}$ | 1.57 and −0.93 | 0.33 and −0.69 | 0.78 and −1.05 | 1.39 and −1.19 | 0.92 and −1.36 |

temperatures, ranging from 400 to 1100 K and pressures up to 2000 atm.[8] Nine compositions were studied with $x=0.0$, 0.20, 0.25, 0.30, 0.40, 0.50, 0.60, 0.80, and 1.00. Just the samples with $x=0.0$, 0.2, 0.5, 0.8, and 1.0 were used in the x-ray experiments.

All XRD measurements were performed at room temperature on an Enraf-Nonius Kappa-CCD diffractometer with graphite monochromated Mo $K\alpha$ ($\lambda=0.710\,73$ Å) radiation. Data were collected up to 60° in $2\theta$, with a minimal redundancy of 4. The final unit-cell parameters were based on all reflections. Data collections were made using the COLLECT program (Enraf-Nonius, 1997–2000);[10] integration and scaling of the reflections were performed with the HKL Denzo-Scalepack system of programs.[11] Absorption corrections were carried out using the multiscan method.[12] The structures were solved using Patterson methods with SHELXS-97.[13] The Patterson maps showed all heavy atoms. The fluorine atoms were found in successive difference Fourier maps. The models were refined by full-matrix least-squares procedures on F$^2$ using SHELXL-97.[14] The program WINGX was used to analyze and prepare the data for publication.[15] Crystal data, data collection procedures, and refinement results are summarized in Table I.

The Raman measurements were performed at 300 and 10 K, using the 514.5-nm line of an argon-ion laser as the excitation source. A near backscattering geometry was used without polarization analysis of the scattered beam. The power was kept in 200 mW and a cylindrical lens was used to avoid overheating of the samples. The spectra were recorded using a U-1000 Jobin-Yvon double-monochromator coupled to a conventional photon counting system and a T64000 Jobin-Yvon coupled to a charge-coupled device (CCD) detector.

## III. RESULTS AND DISCUSSION

### A. X-ray diffraction

Considering the ionic radii of the atoms involved in the chemical formula and the molar fraction of $Sc^{3+}$ and $Ga^{3+}$, it is possible to calculate the Goldschmidt's tolerance factor $t$ for the whole series studied here. For $Cs_2NaGa_xSc_{1-x}F_6$, $t$ and $x$ are linearly related by $t=0.99+0.03x$. Therefore for $0.00<x\leqslant 0.23$ it is expected a cubic structure since $t$ ranges from 0.99 to 1.00. For $0.23<x<1$ a trigonal structure is expected.

The crystal structure of one of the end members, $Cs_2NaScF_6$, which was determined in the $Fm3m$ space group,[2] is shown in Fig. 1. In spite of the structure being well known, we decided to perform its determination in order to compare it with the other crystal phases in analogous experimental conditions. Our measurement confirmed the cubic structure (see Table I), as pointed out by the tolerance factor predictions ($t=0.99$) and also the early study performed by Sheneider and Hoppe.[2] On the other hand, the structure of the other end member, $Cs_2NaGaF_6$, was unknown yet. Its tolerance factor, $t=1.02$, points to a trigonal structure, which was confirmed by our x-ray data: the structure was determined in the $R3m$ space group. The schematic structure of the $Cs_2NaGaF_6$ is given in Fig. 2 and the structural param-

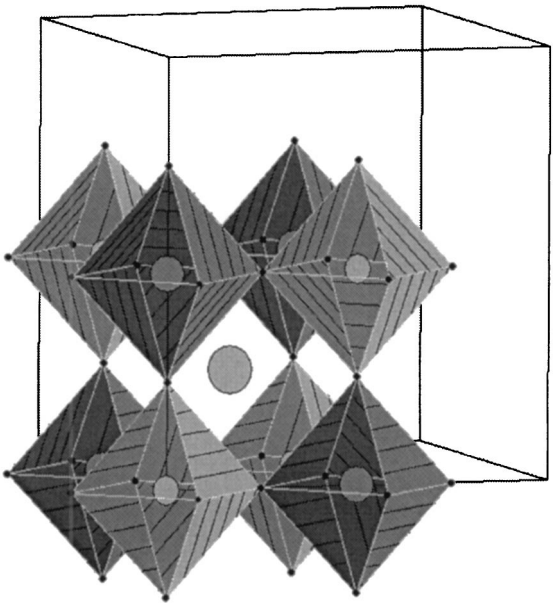

FIG. 1. $Cs_2NaScF_6$ schematic structure showing the Na (dark gray) and Sc (light gray) octahedrons. The Cs atom is the light gray sphere surrounded by the octahedrons. $-1/4<x<3/4$; $-1/4<y<3/4$; $-1/4<z<3/4$ is shown.

eters in Table I. For these two end members of the series, these indications are in good agreement with our Raman spectroscopy results.

The crystal structure of the compositions closer to the end members, $x=0.2$ ($t=0.996$) and 0.8 ($t=1.014$), was successfully determined in the space groups $Fm\bar{3}m$ and $R\bar{3}m$, respectively, confirming the predictions of the tolerance factor. Our x-ray data show that the structure for $x=0.5$ ($t=1.005$) is isostructural to the end member $Cs_2NaGaF_6$. The fractional coordinates, thermal displacement parameters, and site occupancy of all phases are shown in Tables II and III.

Let us discuss first the cubic structures ($x=0.0$ and 0.2). The main geometric parameters for these samples are given in Table IV. In these structures, the $Sc^{3+}$ and $Na^{+}$ cations are octahedrally coordinated by six fluorine atoms. For each octahedron, the six $M-F$ bond lengths are equivalent. The $Cs^{+}$ cations are coordinated to 12 fluorine atoms, all of them at the same distance. For $x=0.2$, since the $Ga^{3+}$ (ionic radii $=0.76$ Å) substitute $Sc^{3+}$ (ionic radii$=0.885$ Å) in the $M$ site, the $M-F$ bond length is expected to decrease. In fact the $M-F$ bonds decreases slightly from $x=0.0$ [2.041(6) Å] to $x=0.2$ [2.023(3) Å]. The bonds Cs–F and Na–F, remain almost equivalent for $x=0.0$ and $x=0.2$. The occupancy of the $M$ site, shared by the $Sc^{3+}$ and $Ga^{3+}$ ions, in $x=0.2$ was refined and their values converged to the nominal value. Therefore $x$ was constrained to be exactly 0.2 in the final refinements. The difference Fourier maps found the fluorine atoms occupying the 24($e$) Wyckoff position.

In the trigonal side of the studied series for the $x=0.5$ and 0.8 compositions, there was observed an ordering of $Sc^{3+}$ and $Ga^{3+}$ cations between the 3($a$) and 3($b$) sites which were labeled as $M1$ and $M2$ (see Table III). A special linear restraint was used during the least-square refinements in order to determine quantitatively the cation distribution.

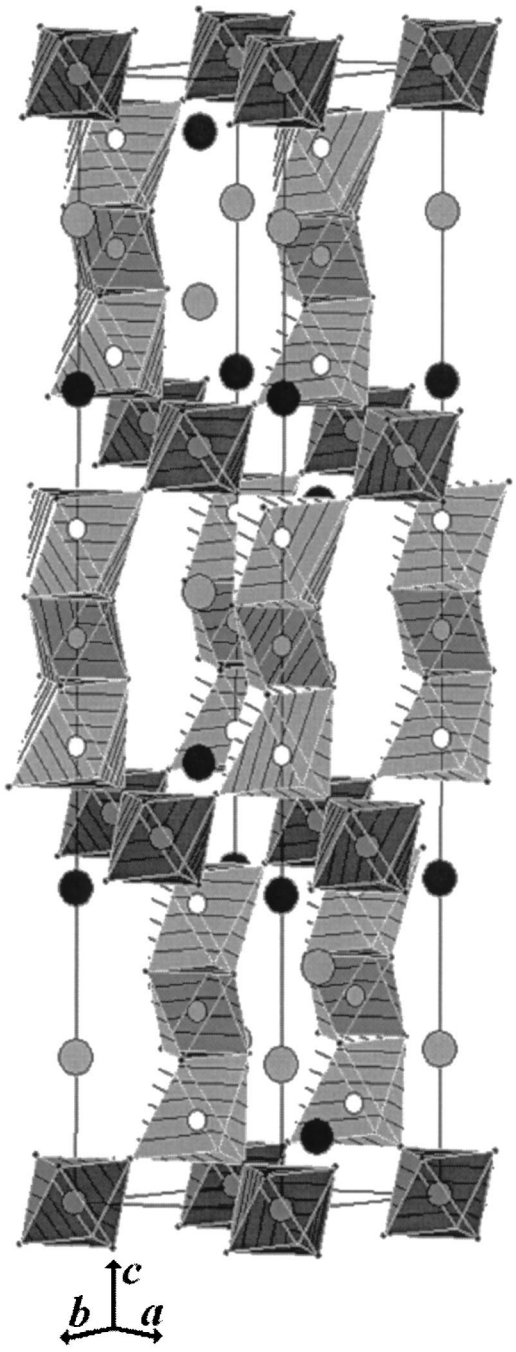


FIG. 2. $Cs_2NaGaF_6$ schematic structure showing the Ga(1) (dark gray), Ga(2) (medium gray), and Na (light gray) octahedrons. Some Cs atoms are shown as spheres in black [Cs(1)] and in light gray [Cs(2)]. Some of the octahedra were omitted for clarity.

The restraint used allowed the distribution of $Ga^{3+}$ and $Sc^{3+}$ over $M1$ and $M2$ sites so that the elemental composition corresponds (within suitable standard deviation) to the nominal one. The restraint also kept the sum of site occupation factors constant and equal to 1 during the refinements. As shown in Fig. 3, the $M1F(2)_6$ unit is a corner-sharing octahedron, whereas the $M2F(1)_6$ unit is a face-sharing octahedron. Therefore metal-metal repulsion is stronger in the $M2$ than in the $M1$ site. In this way, it is reasonable to expect that the bigger cations occupy preferentially the $M1$ site. In fact, our cation distribution model shows that the $Sc^{3+}$ cat-

TABLE II. Atomic coordinates, occupation (Oc) and equivalent isotropic displacement parameters ($Å^2\times10^3$) for the cubic phases ($x=0.0$ and $x=0.2$). $U$(eq) is defined as one third of the trace of the orthogonalized $U^{ij}$ tensor.[i] $x=y=z=1/4$;[ii] $x=y=z=1/2$;[iii] $x=y=z=0$;[iv] $y=z=0$.

| Site | Symmetry | Atom | Fractional coordinates, $U$(eq) and Oc | ($x=0$) | ($x=0.2$) |
|---|---|---|---|---|---|
| $A$ | $8(c)\ \bar{4}3m$ | $Cs^{i}$ | $U$(eq) | 31(1) | 19(1) |
| $B$ | $4(b)\ m\bar{3}m$ | $Na^{ii}$ | $U$(eq) | 29(1) | 16(1) |
| $M$ | $4(b)\ m\bar{3}m$ | Sc, $Ga^{iii}$ | $U$(eq) | 26(1) | 17(1) |
| | | | $Oc_{Sc}$ | 1 | 0.8 |
| | | | $Oc_{Ga}$ | 0 | 0.2 |
| $X$ | $24(e)\ 4m\cdot m$ | $F^{iv}$ | $x$ | 0.2302(7) | 0.2287(3) |
| | | | $U$(eq) | 32(2) | 21(1) |

ion, which has bigger ionic radii than the $Ga^{3+}$, has a strong preference to occupy the $M1$ site instead the $M2$ one (see Table III).

The main geometric parameters of the trigonal phases are given in Table IV. The $M1F(2)_6$ and $M2F(1)_6$ units present slightly distorted octahedral geometry. Due to the symmetry of the $3(a)$ and $3(b)$ sites, both octahedrons present equivalent Ga–F bond lengths. Comparing the bond angles of each unit it is observed that for all trigonal phases the $M2F(1)_6$ octahedron is slight more distorted than $M1F(2)_6$ one. These differences are due to the fact that the $M1F(2)_6$ unit forms a corner-sharing octahedron, whereas the $M2F(1)_6$ one forms a face-sharing octahedron. For $x=1.0$ the $M1-F(2)$ and $M2-F(1)$ bond lengths present quite similar values. However, for the trigonal phases, rich in $Sc^{3+}$, the $M1-F(2)$ bond length is expected to be longer than the $M2-F(1)$ one, since the $Sc^{3+}$, which is bigger than $Ga^{3+}$, prefers to occupy the $M1$ site, as pointed out by our occupancy refinements. In fact, it was observed that both

TABLE IV. Geometric parameters (Å) of the series $Cs_2NaGa_{0.5}Sc_{0.5}F_6$.

| | $x=0.0$ | $x=0.20$ | $x=0.50$ | $x=0.80$ | $x=1.0$ |
|---|---|---|---|---|---|
| Cs–F | 3.1398(5) | 3.1332(2) | | | |
| $Cs(1)-F(1)^{up}$[a] | | | 3.129(4) | 3.119(2) | 3.120(3) |
| $Cs(1)-F(1)^{equatorial}$ | | | 3.1692(3) | 3.1443(3) | 3.1415(4) |
| $Cs(1)-F(2)^{down}$ | | | 3.269(4) | 3.217(3) | 3.211(3) |
| $Cs(2)-F(1)^{down}$ | | | 3.142(3) | 3.129(3) | 3.119(3) |
| $Cs(2)-F(2)^{up}$ | | | 3.429(4) | 3.380(3) | 3.360(3) |
| $Cs(2)-F(2)^{equatorial}$ | | | 3.2011(6) | 3.1785(5) | 3.1790(6) |
| Na–F | 2.392(6) | 2.400(3) | | | |
| Na–F(1) | | | 2.377(5) | 2.364(4) | 2.371(4) |
| Na–F(2) | | | 2.239(4) | 2.263(3) | 2.278(4) |
| $M$–F | 2.041(6) | 2.023(3) | | | |
| $M(1)$–F(2) | | | 2.006(4) | 1.933(3) | 1.905(3) |
| $M(2)$–F(1) | | | 1.915(3) | 1.896(3) | 1.904(3) |
| $M$–Na | 4.4332(4) | 4.4235(5) | | | |
| $M(1)$–Na | | | 4.235(4) | 4.186(3) | 4.172(4) |
| $M(2)$–Na | | | 2.966(4) | 2.954(3) | 2.963(4) |

[a]See also Fig. 3.

$M1-F(2)$ and $M2-F(1)$ bond lengths increase with the increasing of $Sc^{3+}$ content in the trigonal side of the compositional series, that means from $x=1.0$ to $x=0.5$ samples. However, the increase rate of the $M1-F(2)$ bond is bigger than the $M2-F(1)$ one. For $x=0.5$ the difference reaches the maximum: the $M1-F(2)$ is 2.006(4) Å and $M1-F(2)$ is 1.915(3) Å.

The distortion of the $NaF_6$ octahedron is very strong and is independent of the composition. In Fig. 3 we can also see that Na cations are displaced, along the $c$ axis, to up and to down in relation to the $M2$ site. These displacements occur in order to minimize the repulsion of the face-sharing octahedral triad Na–$M2$–Na. This has a direct effect on the large deviation from 90° of the F–Na–F bond angles from

TABLE III. Atomic coordinates, occupation (Oc) and equivalent isotropic displacement parameters ($Å^2\times10^3$) for the trigonal phases ($x=0.5$, $x=0.8$, and $x=1$). $U$(eq) is defined as one-third of the trace of the orthogonalized $U^{ij}$ tensor.[i] $x=y=0$;[ii] $x=y=z=0$;[iii] $x=y=0$, $z=1/2$.

| Site label | Site symmetry | Atom | | $x=0.5$ | $x=0.8$ | $x=1.0$ |
|---|---|---|---|---|---|---|
| $A_1$ | $6(a)\ 3m$ | $Cs^{i}$ | $z$ | 0.1289(1) | 0.1283(1) | 21(1) |
| | | | $U$(eq) | 21(1) | 23(1) | 22(1) |
| $A_2$ | $6(a)\ 3m$ | $Cs^{i}$ | $z$ | 0.2797(1) | 0.2805(1) | 0.2808(1) |
| | | | $U$(eq) | 24(1) | 26(1) | 24(1) |
| $B$ | $6(b)\ 3m$ | $Na^{i}$ | $z$ | 0.4035(1) | 0.4028(1) | 0.4022(1) |
| | | | $U$(eq) | 19(1) | 23(1) | 20(1) |
| $M_1$ | $3(a)\ \bar{3}m$ | Ga,$Sc^{ii}$ | $U$(eq) | 26(1) | 15(1) | 15(1) |
| | | | $Oc_{Sc}$ | 0.8 | 0.676(8) | 0 |
| | | | $Oc_{Ga}$ | 0.2 | 0.324(8) | 1 |
| $M_2$ | $3(b)\ \bar{3}m$ | Ga,$Sc^{iii}$ | $U$(eq) | 26(1) | 16(1) | 17(1) |
| | | | $Oc_{Sc}$ | 0.2 | 0.924(8) | 0 |
| | | | $Oc_{Ga}$ | 0.8 | 0.076(8) | 1 |
| $X_1$ | $18(h)\cdot m$ | F | $x$ | 0.1402(3) | 0.1398(2) | 0.1404(3) |
| | | | $y$ | −0.1402(3) | −0.1398(2) | −0.1404(3) |
| | | | $z$ | 0.4627(1) | 0.4625(1) | 0.4622(1) |
| $X_2$ | $18(h)\cdot m$ | F | $x$ | 0.1824(3) | 0.1868(2) | 0.1884(3) |
| | | | $y$ | −0.1824(3) | −0.1868(2) | −0.1884(3) |
| | | | $z$ | 0.6296(1) | 0.6304(1) | 0.6311(1) |
| | | | $U$(eq) | 27(1) | 28(1) | 25(1) |

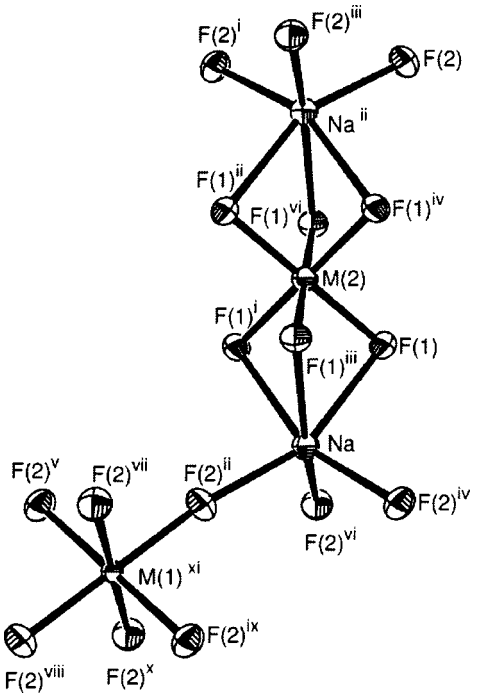


FIG. 3. ORTEP-3 view showing the octahedral neighborhood of the $M(1)$, $M(2)$, and Na sites. Symmetry codes: $^{i}-y,x-y,z$; $^{ii}y,x,-z+1$; $^{iii}-x+y,-x,z$; $^{iv}-x,-x+y,-z+1$; $^{v}-x,-x+y+1,-z+1$; $^{vi}x-y,-y,-z+1$; $^{vii}x-y-1,-y,-z+1$; $^{viii}x-2/3,y+2/3,z-1/3$; $^{ix}-y-2/3,x-y-1/3,z-1/3$; $^{x}-x+y+1/3,-x+2/3,z-1/3$; $^{xi}x-1/3,y+1/3,z+1/3$.

$\sim 67°$ to $102°$. Due to the same reason, the Na–F(1) bond length is $\sim 0.1$ Å longer than the Na–F(2) one, which again is independent of the composition.

In Fig. 4 is shown the coordination environment of the $Cs^+$ cations in the trigonal phase. The two independent sites, Cs1 and Cs2, have coordination number equal to 12. However, for both sites, just three Cs–F separations are symmetrically independent (Table IV).

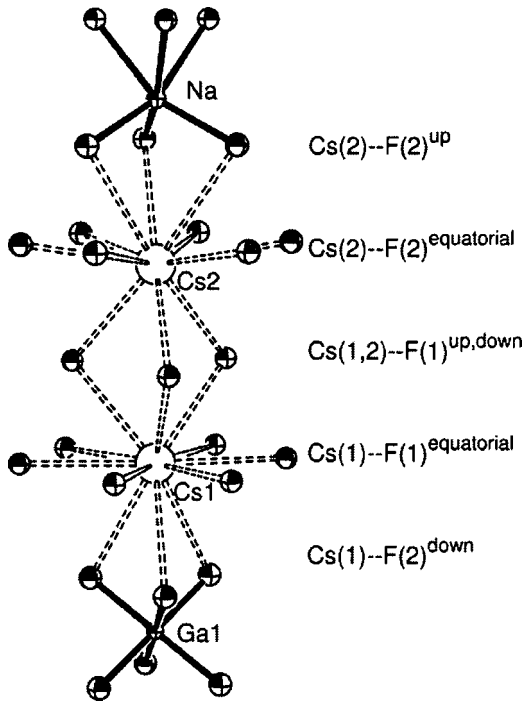


FIG. 4. ORTEP-3 view showing the neighborhood of the $A(1)$ and $A(2)$ sites occupied by Cs(1) and Cs(2) atoms, respectively.

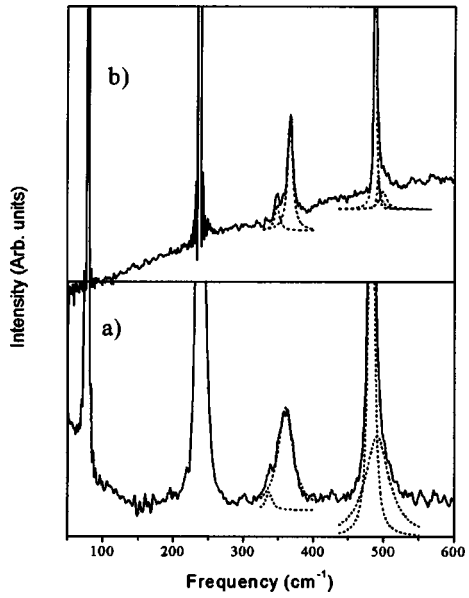


FIG. 5. Comparison of the $Cs_2NaScF_6$ Raman spectra at different temperatures: (a) 300 K and (b) 10 K. Dot-dashed lines represent fitting curves.

### B. Raman scattering

For $Cs_2NaScF_6$, whose symmetry is $Fm\bar{3}m$ $(O_h^5)$, the group theory predicts four Raman-active modes of symmetry $1A_{1g}+1E_g+2F_{2g}$. Our experimental results at room temperature seems agree with the group theory predictions: the depolarized Raman spectrum shows four peaks at 75, 240, 360, and 490 $cm^{-1}$, as it can be seen in Fig. 5(a). However, at low temperature (10 K), the more resolved Raman spectrum shows that in fact both peaks at about 360 and 490

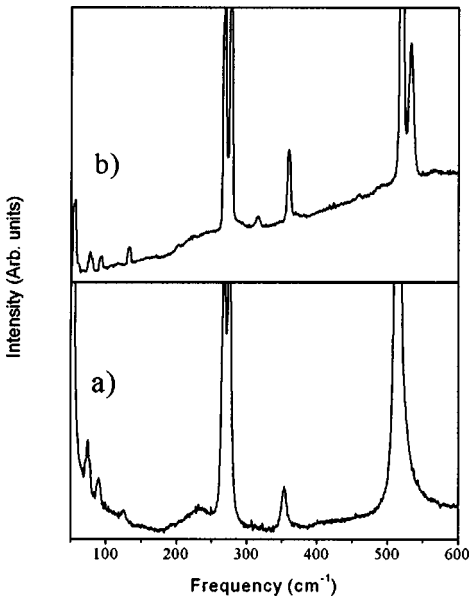


FIG. 6. Comparison of the $Cs_2NaGaF_6$ Raman spectra at different temperatures: (a) 300 K and (b) 10 K.

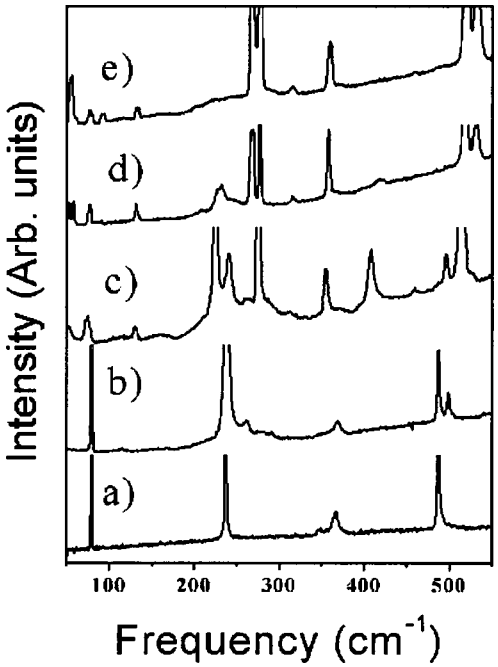


FIG. 7. Evolution of the Raman spectra of the $Cs_2NaGa_xSc_{1-x}F_6$ at 10 K: (a) $x=0.0$, (b) $x=0.2$, (c) $x=0.5$, (d) $x=0.8$, and (e) $x=1.0$.

$cm^{-1}$ present side bands at 355 and 492 $cm^{-1}$, respectively, displayed in Fig. 5(b). Similar result for the higher frequency band was observed in Ref. 16, which the authors attributed to a local mode associated to the presence of $Cr^{3+}$ impurity at the $Al^{3+}$ site.

On the other end of the series, $Cs_2NaGaF_6$ crystallizes in the trigonal space group $R\bar{3}m$ $(D_{3d}^5)$ for which the group theory predict 16 Raman active modes of symmetry $7A_{1g}+9E_g$. Although at room temperature it is difficult to identify all peaks, the Raman spectrum at 10 K shows at about 16 peaks, as displayed in Figs. 6(a) and 6(b). Figure 7 displays the evolution of the phonon spectra as a function of gallium concentration, from the cubic to trigonal phase.

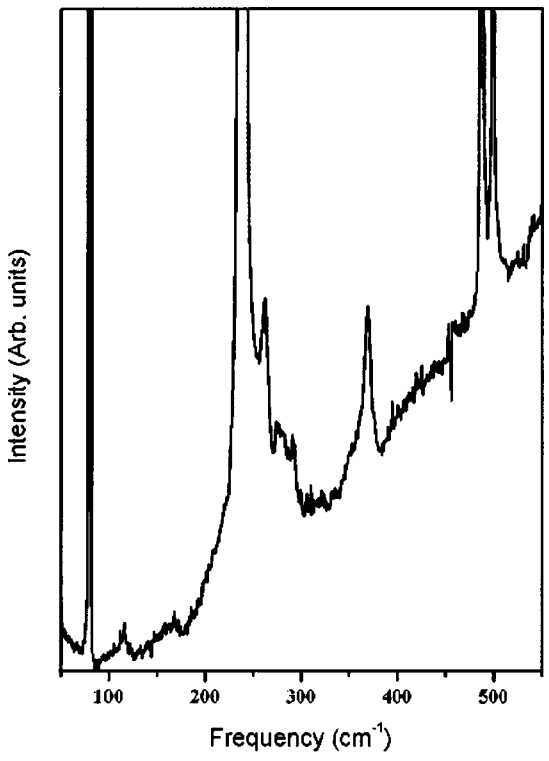


FIG. 8. Raman spectrum of the $Cs_2NaGa_{0.2}Sc_{0.8}F_6$ at 10 K.

Figure 8 shows the Raman spectrum at 10 K for $x=0.2$. Although the XRD results indicate no changes in the overall lattice symmetry, the Raman spectrum shows clearly the presence of new peaks. This may be explained considering that the vibrational spectrum of a solid solution is strongly dependent of the specie of the atomic substitution, involving atoms with different masses and chemical characteristics. In cases where the chemical bonds are predominantly covalent (short range), it can be expected that the substitutional cation forms a sublattice which may vibrates at different frequencies of the host lattice, leading to the so-called two-mode behavior. On the other hand, if the chemical bonds are predominantly ionic (long range), all atoms are forced to vibrate at the same frequency, leading to a one-mode behavior of the vibrational spectrum if the site symmetry does not change. In the present case, all bonds are strongly ionic, so it is expected an one mode behavior relationship to the frequency shifts and a simultaneous change in the number of the phonon modes due to the structural phase transition. However, the XRD measurements indicate no structural phase transition for this Ga concentration, but changes in Ga–F and Sc–F bond lengths. These local changes are than responsible for the changes in the phonon spectrum. Furthermore, the XRD results show a cubic $Fm\bar{3}m$ symmetry to $x=0.0$ and 0.2, and a trigonal $R\bar{3}m$ symmetry to $x=0.5$, 0.8, and 1.0. So the extra peaks in the Raman spectra of all these samples can be attributed to the local changes in the site symmetry, only detected by Raman scattering, a local probe, contrary to XRD that gives the average atom distribution in the crystal. This effect was already observed in $ABO_3$-type perovskites such as $BaTiO_3$, where the transition metal is within an oxygen octahedron. Perovskites often exhibit local structures that show less symmetry than the global symmetry determined by classic XRD.[17,18] The side bands of the peaks at 355 and 492 $cm^{-1}$ for $x=0$, atributed to impurities in Ref. 16, show a clear evolution in the Raman spectrum of sample $x=0.2$, mainly at low temperature. These ''sidebands'' are, then, due to local distortion that exists since $x=0$.

At intermediary concentrations the Raman spectra show practically all modes of the trigonal phase, with the frequencies changing due to the cationic substitution, corroborating the one-mode behavior, as displayed in Fig. 9.

## IV. CONCLUSIONS

Raman scattering and x-ray-diffraction measurements allowed us to characterize in detail the structural phase transition of the series $Cs_2NaGa_xSc_{1-x}F_6$ solid solutions for the complete range of Ga concentration. For $x=0$, the XRD data confirm the cubic $Fm\bar{3}m$ space group, while for $x=1$ they indicate a trigonal space group $R\bar{3}m$. For intermediate $x$ values the XRD data point out the cubic $Fm\bar{3}m$ space group for

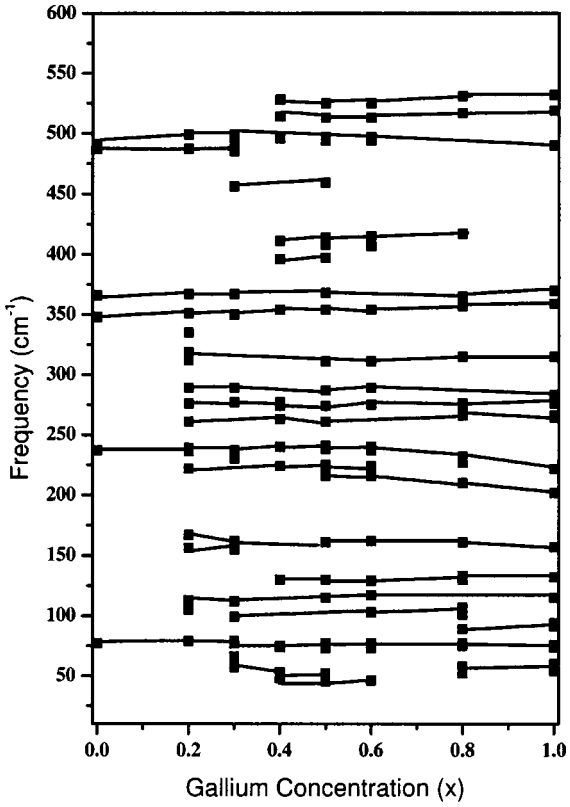


FIG. 9. Variation frequency modes as a function of Ga concentration at 10 K.

the sample with $x=0.2$ and the trigonal $R\bar{3}m$ for those with $x=0.5$ and 0.8. Therefore the XRD data show that the structural phase transition occurs between $x=0.2$ and 0.5. For the end members, these results agree with the Raman data: four Raman-active modes were identified for the sample with $x=0$ (cubic structure) and about 16 Raman-active modes for the sample with $x=1$ (trigonal structure). The vibrational spectra evolution with the cation substitution shows a mixed behavior due to simultaneous local symmetry changes, structural phase transition, and frequency shifts, characteristics of the one-mode behavior. These three simultaneous effects are only observed in the Raman scattering since it is a short-range probe, opposite to the XRD, an average long-range probe. Furthermore, the results showed that since low Ga concentrations, $x=0.2$, the Raman spectrum shows new peaks, starting to acquire the trigonal end-member characteristics, although the XRD results still indicate cubic lattice symmetry. These new Raman modes at low Ga concentration were attributed to local symmetry changes, indicating that the cubic-to-trigonal phase transition starts from local changes but preserving the overall symmetry, changing to new overall symmetry at higher ($x=0.5$) gallium contents. These local changes denounced by Raman scattering may be important from the applications point of view, since they influence directly the crystal field, which determines the electronic energy levels of dopants for application in the manufacturing solid-state lasers.

## ACKNOWLEDGMENTS

The authors wish to thank N. M. Khaidukov for growing the samples. This work was partially supported by the Brazilian research-financing institutions FAPESP, CNPQ, and CAPES.

[1] E. G. Steward and H. P. Rooksby, Acta Crystallogr. **6**, 49 (1953).
[2] S. Sheneider and R. Hoppe, Z. Anorg. Allg. Chem. **376**, 168 (1970).
[3] R. Haegele, W. Verscharen, and E. Babel, Z. Naturforsch. B **30**, 346 (1975).
[4] D. Babel, Struct. Bonding (Berlin) **3**, 1 (1967).
[5] D. Babel, Z. Anorg. Allg. Chem. **51**, 33 (1995).
[6] D. Babel, R. Haegele, G. Pausewan, and F. Wall, Mater. Res. Bull. **8**(12), 1371 (1973).
[7] I. N. Felrov, M. V. Gorev, K. S. Aleksandrov, A. Tressaud, J. Grannec, and M. Couzin, Mater. Sci. Eng., R. **24**(3), 81 (1998).
[8] R. J. M. da Fonseca, A. D. Tavares, Jr., P. S. Silva, T. Abritta, and N. M. Khaidukov, Solid State Commun. **110**, 519 (1999).
[9] C. L. de Barros, R. B. Barthem, and N. M. Khaidukov, J. Lumin. **82**, 307 (1999).
[10] Enraf-Nonius (1997–2000), COLLECT, Nomuis BV, Delft, the Netherlands.
[11] Z. Otwinowski and W. Minor, in *Methods in Enzymology*, edited by C. W. Carter, Jr. and R. M. Sweet (Academic Press, New York, 1997), Vol. 276, pp. 307.
[12] R. H. Blessing, Acta Crystallogr., Sect. A: Found. Crystallogr. **A51**, 33 (1995).
[13] G. M. Sheldrick, *SHELXL-97*, *Program for Crystal Structure Analysis*, University of Gottingen, Gottingen, Germany, 1997.
[14] G. M. Sheldrick, *SHELXS-97*, *Program for Crystal Structure Analysis*, University of Gottingen, Gottingen, Germany, 1997.
[15] L. J. Farrugia and G. X. Win, J. Appl. Crystallogr. **32**, 837 (1999).
[16] H. N. Bordallo, R. W. Henning, L. P. Sosman, R. J. M. da Fonseca, A. D. Tavares, Jr., K. M. Hanif, and G. F. Strouse, J. Chem. Phys. **115**, 4300 (2001).
[17] R. Comes, M. Lambert, and A. Guinier, Solid State Commun. **6**, 715 (1968).
[18] N. Sicron, B. Ravel, Y. Yacoby, E. A. Stern, F. Gogan, and J. J. Rehr, Phys. Rev. B **50**, 13 168(1994).